High-Performance Nanowire Hydrogen Sensors by Exploiting the Synergistic Effect of Pd Nanoparticles and Metal–Organic Framework Membranes

Matthieu Weber, Jae-Hun Kim, Jae-Hyoung Lee, Jin-Young Kim, Igor Iatsunskyi, Emerson Coy, Martin Drobek, Anne Julbe, Mikhael Bechelany, Sang Sub Kim

High Performance Nanowires Hydrogen Sensors by Exploiting the Synergistic Effect of Pd Nanoparticles and MOF Membranes

Matthieu Weber,[†,‡] Jae-Hun Kim,[†,§] Jae-Hyoung Lee,[§] Jin-Young Kim,[§] Igor Iatsunskyi,[×] Emerson Coy,[×] Martin Drobek,[‡] Anne Julbe,[‡] Mikhael Bechelany,[*,‡] and Sang Sub Kim[*,§]

[‡] *Institut Européen des Membranes, IEM – UMR 5635, ENSCM, CNRS, University of Montpellier, Place Eugène Bataillon, 34095 Montpellier cedex 5, France.*

[§] *Department of Materials Science and Engineering, Inha University, Incheon 22212, Republic of Korea.*

[×] *NanoBioMedical Centre, Adam Mickiewicz University in Poznan, 61-614, Umultowska str. 85 Poznan, Poland.*

[†] *co-first authors*

KEYWORDS. ZnO nanowire, Pd nanoparticle, ALD, ZIF-8 nanomembrane, encapsulation, gas sensing, molecular sieving.

ABSTRACT. Herein, we report the fabrication of hydrogen gas sensors with enhanced sensitivity and excellent selectivity. The sensor device is based on the strategic combination of ZnO nanowires (NWs) decorated with palladium nanoparticles (Pd NPs) and a molecular sieve metal organic framework (MOF) nanomembrane (ZIF-8). The Pd NPs permit the sensors to reach maximal signal responses, whereas the ZIF-8 overcoat enables for an excellent selectivity. Three steps were employed for the fabrication: *i)* coating of a miniaturized sensor with vapor grown ZnO NWs, *ii)* decoration of these NWs with Pd NPs by atomic layer deposition (ALD), and *iii)* partial solvothermal conversion of the

tuned NWs surface to ZIF-8 nanomembrane. The microstructure and composition investigations of the ZIF-8/Pd/ZnO nanostructured materials confirmed the presence of both metallic Pd NPs and uniform ZIF-8 thin membrane layer. The integration of these nanomaterials within a miniaturized sensor device enabled the assessment of their performance for H_2 detection at concentrations as low as 10 ppm in the presence of various gases such as C_6H_6, C_7H_8, C_2H_5OH and CH_3COCH_3. Remarkably high response signals of 3.2, 4.7 and 6.7 (R_a/R_g) have been measured for H_2 detection at only 10, 30 and 50 ppm, whereas no noticeable response towards other tested gases was detected, thus confirming the excellent H_2 selectivity obtained with such sensor design. The results obtained showed that the performance of gas sensors towards H_2 gas can be greatly increased by both the addition of Pd NPs and the use of ZIF-8 coating acting as a molecular sieve membrane. Furthermore, the presented strategy could be extended towards the sensing of other species by a judicious choice of both the metallic NPs and MOFs materials with tuned properties for specific molecules detection, thus opening a new avenue for the preparation of highly selective sensing devices.

TOC

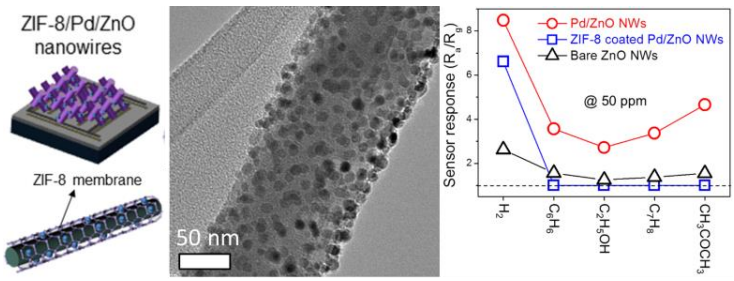

1. INTRODUCTION

An efficient monitoring of hydrogen gas is vital in many chemical processes, such as the synthesis of ammonia or the hydration of hydrocarbons. Moreover, hydrogen is also considered as one of the best clean energy carriers which could contribute to tackle the major environmental issues our society is facing.[1-4] Therefore, the development of reliable, fast and precise hydrogen sensors is of great importance for hydrogen production, storage and use.[3]

The efficiency of a gas sensor is mainly related to its sensitivity and selectivity, but other parameters such as the response and recovery times, or the stability over time also play an essential role in the gas sensing performance. Typically, the sensing mechanism involves the adsorption of gases onto the surface of the functional material, leading to a change in its electrical conductivity. In this respect, the most widely applied sensor materials are nowadays based on semiconductor metal oxides presenting excellent physical and chemical stabilities.[5-14] Furthermore, their low cost and industrial scalability, as well as the large number of gases they can detect, make them attractive for numerous sensing applications.[5] Among the different semiconductor metal oxides, zinc oxide (ZnO) is a material of choice for gas detection, as it typically features excellent physical properties (e.g. crystallinity) and high charge carrier transport properties.[15-17] However, such sensors typically suffer from a relatively low selectivity.[18] Strong efforts are thus required to improve both sensor response intensity and selectivity.

Recently, our research team has reported on an innovative strategy to improve the selectivity of integrated gas sensing devices by overcoating metal oxide nanowires (NWs) with a thin uniform metal organic framework (MOF) permselective nanomembrane (ZIF-8, SIM-1)[19-21] offering molecular sieving properties.[19-20] In particular, the ZIF-8 nanomembrane present micropores of ~0.34 nm allowing hydrogen molecules (kinetic diameter of 0.29 nm) to pass through, whereas larger gas molecules cannot. Koo *et al.* confirmed the efficient use of ZIF-8 nanomembrane to enhance the performance of NWs hydrogen sensors.[22] Despite the good performance measured, further

improvements are still desired to enhance both the gas sensing devices response and selectivity in the presence of interfering reducing gases.

Concerning the detection of hydrogen, one promising strategy is to apply composite materials containing palladium metal nanostructures, in order to increase the gas sensors selectivity towards H_2. In fact, recent studies [4, 6, 23-24] focusing on the synthesis of sensing materials have shown that metal semiconductor NWs decorated with Pd NPs are very promising candidates as highly sensitive hydrogen detectors.[19-20, 25] Indeed, hydrogen has an exceptional affinity towards Pd, which efficiently dissociates H_2 into hydrogen atoms. Additionally, when supported on a semiconductor material, the Fermi level modulation upon chemical adsorption of hydrogen gas on Pd NPs leads to the band diagram modification at the metal–semiconductor interface.[24] Hence, nanostructured materials decorated with Pd nanoparticles may be advantageously applied for gas sensing of hydrogen with accentuated sensitivity resulting from their extremely high surface-to-volume ratio. Pd NPs can be prepared by various synthesis methods, such as impregnation, deposition/precipitation, sol-gel, ion exchange, or gas phase routes.[26-32] A novel promising strategy for the direct growth of metallic nanoparticles is atomic layer deposition (ALD), a vapor phase technology typically used for the synthesis of thin films with a thickness controllable at the (sub)nanometer scale. ALD of noble metals enables the preparation of metallic thin films and/or nanoparticles with controlled dimensions at the nanoscale on high aspect ratio substrates, and is thus particularly appropriate for the coating of nanowires.[33-42]

Herein, we present a novel route for the preparation of sensing devices with both enhanced hydrogen sensitivity and selectivity. The sensors considered in this work are based on the combination of ALD palladium NPs decorated ZnO NWs and a permselective nanomembrane overcoat offering molecular sieving properties. The fabrication of such fully integrated sensing devices is based on three consecutive steps: *i)* coating of a miniaturized sensor with a forest of ZnO NWs using a vapor growth route, *ii)* decoration of these NWs with Pd NPs by ALD, and *iii)* partial

solvothermal conversion of such decorated NWs to permselective ZIF-8 top-layer. The prepared Pd NPs decorated ZnO NWs with the ZIF-8 overcoat (ZIF-8/Pd/ZnO) were characterized in terms of their microstructure, composition and performance for hydrogen detection in the presence of interfering gases. The excellent efficiency of this original gas sensing device was confirmed by evidencing both high signal response and excellent selectivity towards hydrogen.

2. EXPERIMENTAL

The synthesis protocol for the preparation of ZIF-8/Pd/ZnO nanocomposite gas sensors has been developed and optimized in order to ensure the obtention of both highly dispersed Pd NPs at the surface of interconnected ZnO NWs and a thin selective ZIF-8 nanolayer homogeneously covering the decorated NWs.

2.1. Fabrication of sensor device structure and growth of ZnO NWs:

Typically, gas sensing elements using semiconductor metal oxides are heterogeneously integrated in a miniaturized package with other silicon-based microelectronic elements for powering and interacting with their environment. Therefore, the sensing device considered in this work has been fabricated using conventional microelectronic manufacturing methods in order to allow its future integration. First, an interdigital electrode (IDE) has been designed and fabricated on SiO_2 (200 nm thick)-grown Si (100) substrates using a conventional lithography process. The IDE consisted of tri-layers: Au (3 nm)/Pt (100 nm)/Ti (50 nm) films that were deposited sequentially by using sputtering processes. As already reported in our previous works, the Au was used for its catalytic properties, the Pt layer served as an electrical pathway and the Ti layer was employed to enhance the adhesion between the Si substrate and the Pt layer.[43] The sensor samples consist of 20 electrode pads with each pad being 1.05 mm long and 20 μm wide, the gap between the neighboring electrode pads being 10 μm.

Finally, the sensor device was coated with three-dimensional interwoven mat of interconnected ZnO NWs grown selectively on the Au layer, which fulfilled a catalytic role. The growth of ZnO NWs has been conducted by loading the IDE patterned sensor in a furnace with Zn powders and constant Ar and O_2 flows at a temperature of 950 °C for 1 h.

2.2 ALD of Pd NPs on the ZnO NWs:

In this work, the highly dispersed Pd NPs were synthesized by applying 100 ALD cycles in a low-pressure hot-wall (home-built) ALD reactor. The typical ALD cycle consisted of 5 s pulse of $Pd(hfac)_2$, 15 s exposure, and 10 s purge, followed by a 1 s pulse of formalin, 15 s exposure and 60 s purge with Ar. The bubbler containing the $Pd(hfac)_2$ precursor was heated at 70 °C and the formalin container was kept at room temperature. The deposition chamber was set at a temperature of 220 °C, and the lines were heated at 100 °C to avoid any condensation. Further details about both this deposition protocol and the associated ALD reactor can be found elsewhere.[44-45]

2.3. Synthesis of ZIF-8/Pd/ZnO composite NWs

In order to obtain the selective nanomembrane layer, the ZnO NWs decorated with Pd NPs (Pd/ZnO NWs) were partially converted to a MOF (ZIF-8) layer. For this purpose, the Pd/ZnO NWs were submitted to a solvothermal treatment in a closed pressure vessel (Teflon-lined stainless-steel autoclave – 45 ml) containing 2-methylimidazole (2-mim) dissolved in methanol (2 wt%). The above reaction mixture was prepared under stirring for 10 min to obtain a clear solution.[46] The autoclave was heated in a conventional oven at 100°C for 24 h and then cooled down to room temperature. Finally, the as-obtained ZIF-8/Pd/ZnO NWs were washed several times with methanol and dried at 70°C for 2 h. It should be noted that whereas some previous work focusing on the encapsulation of inorganic NPs within MOF crystals required surface modification with a polymer to prevent NP agglomeration,[47] the low temperature used for growing the MOF in the present work enabled the synthesis of composite sensors without the need of any surface treatment of the NPs.

2.4. Physico-chemical characterizations

Physico-chemical characterizations of nanomaterials (bare ZnO NWs, Pd/ZnO NWs and ZIF-8/Pd/ZnO NWs) have been carried out using various analytical techniques. A high resolution scanning electron microscope (FESEM, Hitachi S-4800) has been used for sample imaging. The samples have also been studied by high-resolution transmission electron microscopy (TEM), using a JEOL ARM 200F at 200 kV equipped with an EDX analyzer. In order to observe the NWs, sample sections were cut using a focused ion beam milling and imaging system (FIB, JEOL JIB-4000). In order to prepare separated NWs for TEM observation, the samples were tilted (60°) and then few FIB milling lines were performed in order to cut NWs out of the surface. Finally, the samples were dipped in ethanol, ultrasonicated for 10-15 min and then 15 µl of the obtained solution were dropped onto a Cu grid. The crystallinity of the synthesized nanomaterials was studied by grazing incidence X-ray diffraction (GIXRD) using a Bruker D5000 (with Cu Kα radiation). The chemical composition of the grown material has been determined by both EDX analysis (Zeiss EVO HD-15) and X-ray Photoelectron Spectroscopy (XPS) (ESCALAB 250 Thermal Electron) with Al-Kα (1486.6 eV). Binding energies were calibrated by using carbon (C 1s = 284.4 eV).

2.5. Sensing measurements

The gas sensing performance of bare ZnO NWs, Pd/ZnO NWs and ZIF-8/Pd/ZnO NWs sensors were studied by exposing the sensors to different gases at various temperatures using a specifically designed sensing system apparatus. The H_2 gas concentration in the sensing measurement chamber was controlled by changing the mixing ratio of the H_2 gas to dry air through accurate mass flow controllers. H_2 gas diluted with dry air (mixture supplied by Daeduk Gas Co., Korea) was used as the H_2 source. To evaluate sensors selectivity, other gases such as toluene (C_7H_8), ethanol (C_2H_5OH), acetone (CH_3COCH_3) and benzene (C_6H_6) were also tested. The sensing response (R) was calculated as $R = R_a/R_g$, where R_a and R_g are the resistances in the absence and in the presence of the target gas, respectively.[48-49]

3. RESULTS AND DISCUSSION

3.1. Synthesis and microstructure of ZIF-8/Pd/ZnO NWs nanosensors

As detailed in the experimental part, the preparation of the novel hydrogen selective gas sensing device (ZIF-8/Pd/ZnO NWs) involves three key steps: i) Growing a network of ZnO NWs on the sensor support; ii) Decorating the NWs with Pd NPs by ALD; iii) Forming a thin ZIF-8 permselective layer by controlled solvothermal conversion of the surface of Pd-decorated ZnO NWs. The three synthesis steps are depicted in Figure 1.

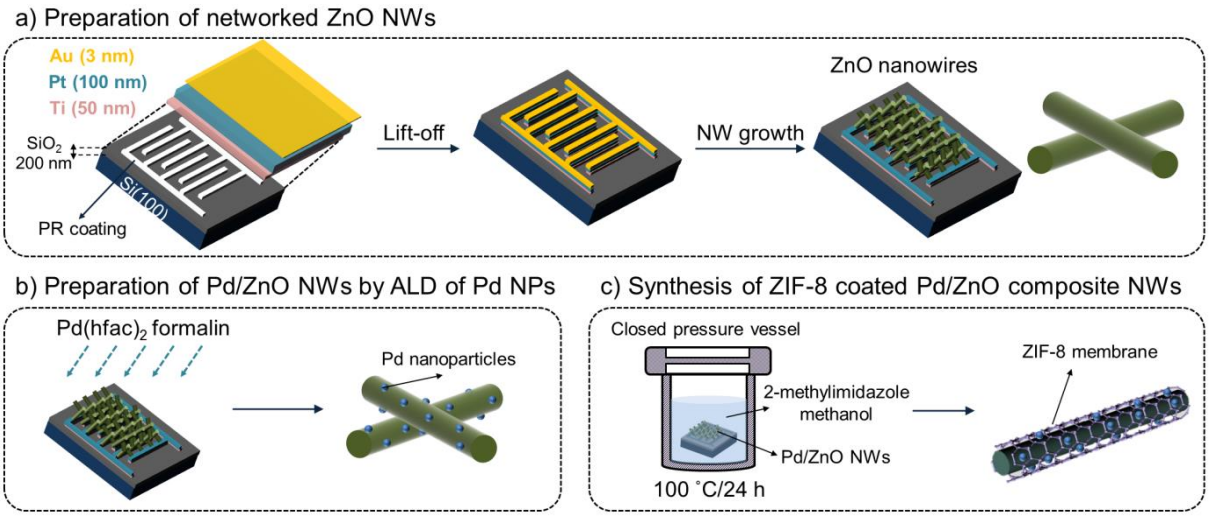

Figure 1. Schematic representation of the 3 key steps enabling the synthesis of the novel gas sensing device.

Typically, gas sensing elements using semiconductor metal oxides are heterogeneously integrated in a miniaturized package with other silicon-based microelectronic elements for powering and interacting with their environment. Therefore, the sensor presented in this work has been fabricated using conventional microelectronic manufacturing methods in order to allow its integration. First, the growth of ZnO NWs has been conducted. The sensing device architecture can be seen in the SEM images displayed in Figure 2a and 2b, where both the entire sensor device and a zoom in are shown.

The ZnO NWs 3D network coating the surface of the sensor pads can be clearly observed in the zoomed image.

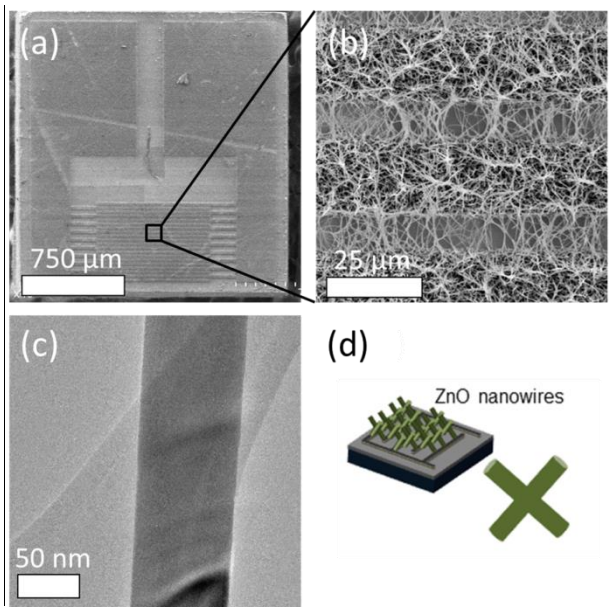

Figure 2. (a,b) SEM images of the entire sensor device and a zoom for visualizing interconnected ZnO NWs on the sensor surface, (c) TEM image of a single ZnO NW, and (d) schematic representation of the bare ZnO NWs sensor.

The connections between the pads ensured by the NWs junctions play an essential role. As shown in the Figure 2, the NWs form a plait-like structure providing electrical pathways whose resistance changes as a function of both the concentration and the nature of the molecules in contact with the sensor device. The synthesized ZnO NWs have random orientation and they are anisotropic in terms of both orientation and growth density. However, it should be noted that this anisotropy does not negatively affect the gas sensing performance. Indeed, it is known that for better gas sensing, higher number of ZnO homojunctions is preferable because it causes more modulation of the resistance. Such a randomly oriented morphology is expected to provide more ZnO homojunctions and thus higher gas response signals. TEM imaging studies have been carried out on the bare ZnO NWs coated devices as well (Figure 2c). The diameter of the observed ZnO NWs was around 80 nm, with lengths

reaching up to 25 µm. It is worth noticing that the sensing properties of such sensors have been reported and described in our previous study.[43]

The second step for the preparation of the novel nanocomposite ZIF-8/Pd/ZnO NWs sensing device involves the synthesis of Pd NPs on ZnO NWs, using ALD. ALD is a vapor phase technique based on self-limiting reactions of precursor molecules with the substrate surface groups, enabling the preparation of nanomaterials controllable at the (sub)nanometer scale.[33, 35, 37] In this work, the ALD process of Pd was based on $Pd(hfac)_2$ and formalin at 220°C. More details are given in the Experimental section. After optimization of the deposition process, it has been found out that 100 ALD cycles lead to the homogeneous deposition of highly dispersed Pd NPs at the surface of ZnO NWs. Palladium having a strong affinity to hydrogen molecules, the addition of Pd NPs on the sensor NWs is expected to result in higher response signals for H_2 detection. Figure 3a and 3b present TEM images showing well dispersed NPs at the surface of the ZnO NWs. The NPs present an average diameter of 6 ± 2 nm and are uniformly dispersed over the whole surface of the NWs.

The presence of Pd NPs was clearly observed by the strong contrast difference between the NPs and the ZnO NW during TEM observation. Additionally, the use of the EDX detector in mapping analysis corroborated the nature of the particles. As shown in Figure 3c, the EDX mapping reveals both a uniform distribution of Zn and O elements corresponding to ZnO NWs and the presence of well dispersed palladium NPs covering homogeneously the NWs surface.

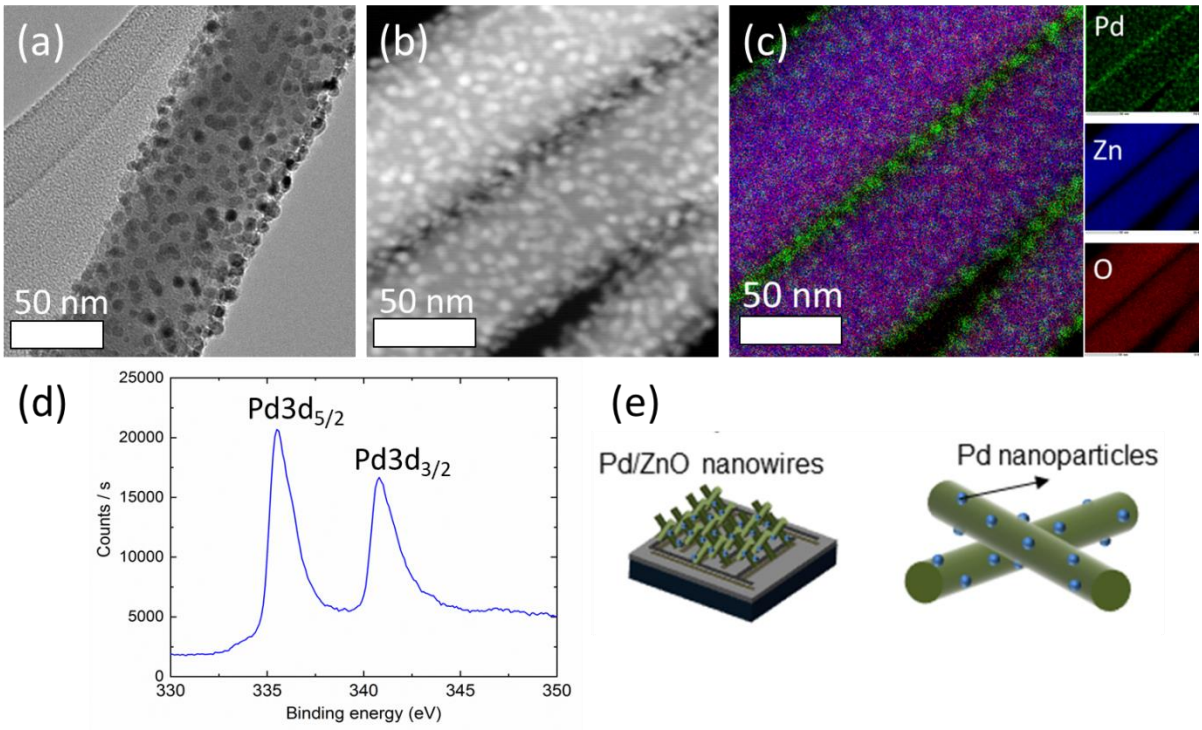

Figure 3. (a) TEM image of a single NW revealing a high dispersion of NPs. (b) SEM image of three NWs decorated with Pd NPs and (c) corresponding EDX mapping. (d) XPS spectra of the Pd 3d scan of the ZnO NWs decorated with Pd NPs. (e) Schematic representation of the Pd/ZnO NWs sensor.

The presence of Pd NPs on the ZnO NWs has been further confirmed by XPS measurements. As expected, the XPS data revealed the presence of metallic palladium, as shown in the Pd 3d scan (Figure 3d). Palladium oxides could not be deconvoluted from the peaks of Pd in the XPS data. Zinc and oxygen elements were also detected by XPS, as the binding energies of O 1s and Zn p3 were found at 532 and 1029 eV, respectively (overall scan is given in Supporting Information S1). A schematic representation of the Pd/ZnO NWs sensor is depicted in Figure 3e.

Next, the solvothermal conversion of the surface of the ZnO NWs decorated with Pd NPs (Pd/ZnO NWs) permitted to fabricate a permselective MOF layer (ZIF-8 nanomembrane). The reaction conditions were selected to achieve the growth of a thin and continuous ZIF-8 layer on the Pd-decorated ZnO NWs while maintaining the NW–NW junction between the electrode pads. The ZIF-8 nanomembrane is supposed to play a role as a permselective barrier increasing the sensor selectivity,

while the ZnO semiconductor core ensures the electrical conductivity of the system. It should be emphasized that this synthesis step is rather challenging, since the surface conversion of the metal oxide NWs has to be sufficient to ensure the homogeneous coverage with the ZIF-8, but not too pronounced in order to preserve the 3D NWs architecture of the sensor support. As discussed in our previous works, the organic ligand (2-mim) coordinates with Zn^{2+} ions during the solvothermal conversion step in order to form the ZIF-8 material at the ZnO NWs surface.[19-21] Considering the low dissociation rate of ZnO to Zn^{2+}, the conversion rate is relatively slow, therefore enabling an accurate control of only the ZnO top-surface conversion to ZIF-8. SEM studies carried out after the solvothermal treatment confirmed the preservation of the interconnected NWs network architecture of the sensors (Figure 4a).The modification of the NWs surface morphology is clearly observed in Figure 4b.

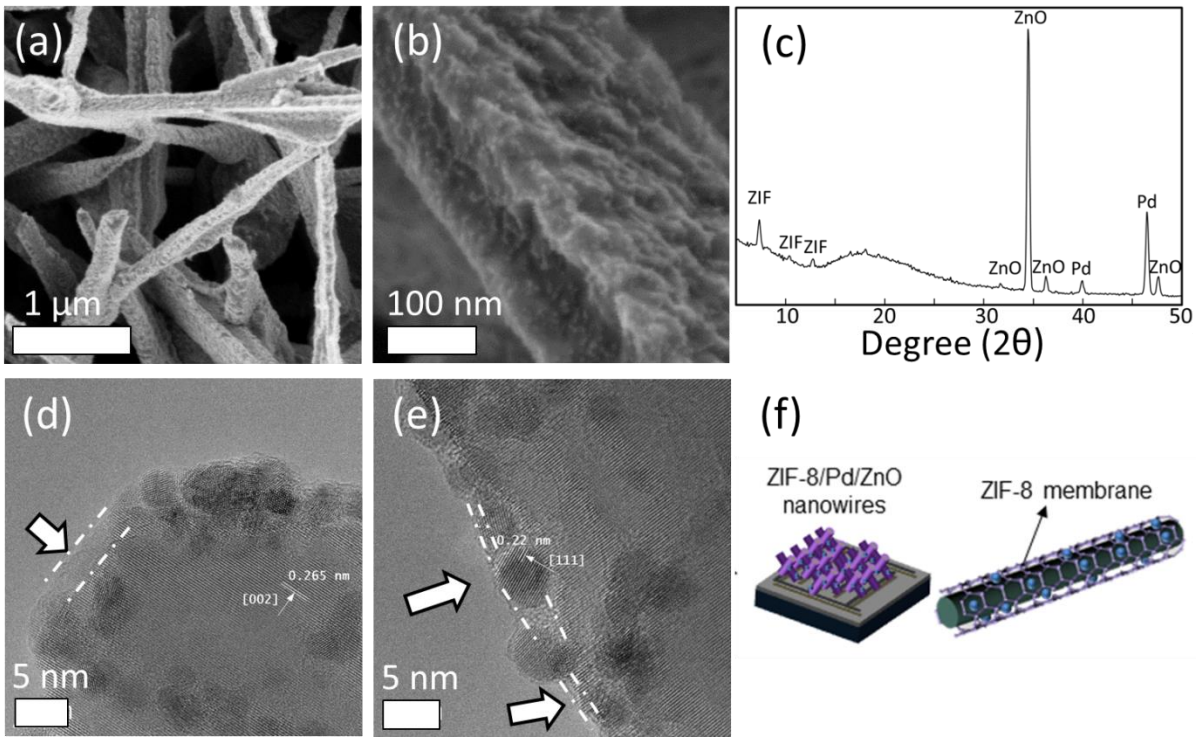

Figure 4. (a,b) SEM images of ZIF-8/Pd/ZnO NWs, (c) GI-XRD diffraction patterns (the ZIF-8, ZnO and Pd peaks are indicated), and (d,e) HRTEM images of the ZIF-8/Pd/ZnO NWs sensing nanomaterial (the

ZIF-8 coating is highlighted). f) Schematic representation of the novel ZIF-8/Pd/ZnO NWs sensor prepared.

High resolution TEM (HR-TEM) imaging using FIB cut sections of the converted Pd/ZnO NWs (ZIF-8/Pd/ZnO NWs) revealed the formation of an ultrathin ZIF-8 layer (2-3 nm thick), homogeneously covering the Pd-decorated NWs surface as highlighted in Figure 4d and 4e. For more clarity, the TEM images with the distribution and the corresponding lattice spacings of the different elements are shown in the Figure S2.

It is expected that the interplay between the properties and interface of the palladium and ZnO materials played a key role upon MOF growth. In fact, the hydroxyl functional groups typically present at oxide surfaces are known to interact with metal ions during MOF growth and to enhance nucleation of MOF crystals on 3D supports such as NW. In addition, the catalytic properties of the noble metal NP is expected to affect MOF growth as well. Although very little is known on that topic former studies suggested that noble metal particles did not compromise the MOF crystallization process.[51-52]

Furthermore, the microstructure of the final composite nanomaterial has been investigated by GI-XRD. The crystallinity of the three components has been clearly evidenced even for such a small amount of material. Indeed, as shown in figure 4c, GI-XRD measurements detected the main diffraction peaks of ZIF-8 (2θ= 7.3° (011), 10.4° (200), 12.7° (112)), ZnO (2θ = 31.7° (100), 34.4° , 36.2°, 47.5°) and Pd (2θ = 40° (111), 47° (200)).[53] Please note that the XRD patterns for the bare ZnO NWs samples are given in Figure S3 (Supporting Information). As discussed in our previous work, the formation of the ZIF-8 material has been confirmed as well by N_2 physisorption measurements featuring values S_{BET} values of about 1760 ± 260 m^2/g.[20] Finally, XPS measurements have been carried out as well for a better understanding of the final sensor composition. As the ZIF-8 was formed (by solvothermal conversion of ZnO) additional elements appeared. Both carbon and nitrogen elements present in the ZIF-8 were clearly detected by XPS, featuring the binding energies of C 1s, O 1s, Zn

2p3, N 1s and Pd 3d at 284.91, 530.87, 1021.66, 399.13 and 346.30 eV, respectively. These results confirmed the formation of the MOF coated Pd/ZnO NWs (Supporting Information S1).

3.2. Sensing measurements:

The sensing device response magnitude and more importantly its selectivity are key parameters in metal oxide-based gas sensors, and too low values strongly limit their practical application. The sensors fabricated in this work were tested for hydrogen detection, from room temperature up to 300°C.

As shown in Figure 5, the response of the sensor based on Pd-decorated ZnO NWs generally presents higher values when compared to the bare ZnO NWs gas sensor (up to a factor 3 at the optimal temperature of 200°C). The thermal stability of the ZIF-8/Pd/ZnO composite material is limited by the stability of its metal-organic part (ZIF-8). The TGA measurements performed on an equivalent ZIF-8/ZnO powder confirmed the excellent material stability up to 400°C (Figure S4), thus making it sufficiently stable for long-term gas sensing experiments at 200°C.

The normalized dynamic resistance curves of the two sensors are shown in the inset of Figure 5, where higher resistance change of Pd/ZnO NWs gas sensor reveals its higher response relative to the bare ZnO NWs gas sensor. Due to their affinity with hydrogen, the Pd NPs effectively enables the corresponding sensor to reach higher signal values for hydrogen sensing. For this Pd/ZnO NWs gas sensing device, the response is initially relatively low, but increases with raising temperature, up to an optimal response value (multiplied by 8) at 200°C, and then decreases for higher temperatures. This is due to the fact that at low temperatures, there is not enough energy for H_2 gas chemisorption by the Pd particles decorating the ZnO NWs of the sensor, whereas at high temperatures (>200°C), the desorption rate is higher than the sorption rate, leading to a low response. In fact, due to its intrinsic properties, palladium can effectively decrease the energy barrier for the sorption of H_2 gas at the ZnO NWs surface. Through the so-called spill-over effect process, the H_2 gas absorbed at the surface of the Pd NPs favors the transfer H atoms to the surface of the ZnO NWs.[54] This process

effectively decreases the optimal sensing temperature of the sensor but also increases its response value. This effect can also be seen in the dynamic resistance curves of bare ZnO and Pd/ZnO NWs gas sensors as a function of sensing temperatures shown in Figures S5 and S6 (Supporting Information). Thus, the Pd NPs effectively enable the sensors to reach intense signal response for H_2 detection.

Apart from sensitivity, the selectivity (or cross-sensitivity) is another key parameter of a gas sensing device. Obviously, if a gas sensor responds to all interfering gases, it cannot precisely detect the desired target gas and fake alarms prohibit their practical use. Thus, the selectivity of both Pd/ZnO and ZIF-8/Pd/ZnO NWs gas sensors was evaluated by exposing the devices to 50 ppm of H_2, C_6H_6, C_7H_8, C_2H_5OH and CH_3COCH_3 gases (at the optimal temperature of 200°C). The dynamic resistance curves are shown in Figure 6a, and Figures 6b and 6c show the corresponding calibration curves of the sensors exposed to H_2 gas and interfering gases, respectively.

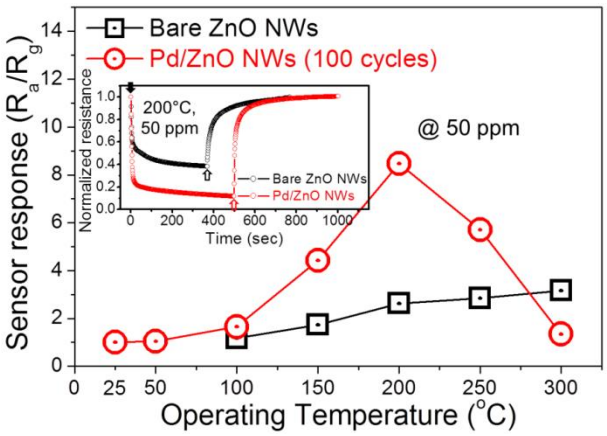

Figure 5. Sensor responses of bare ZnO and Pd/ZnO gas sensors to 50 ppm H_2 gas, as a function of sensing temperature. Inset shows the normalized dynamic resistance curves of bare ZnO and Pd/ZnO gas sensors to 50 ppm H_2 gas at optimal sensing temperature (200°C).

As depicted in Figure 6b, the responses of Pd/ZnO NWs gas sensor to 10, 30 and 50 ppm H_2 gas are 4.3, 6.3 and 8.5 respectively and the responses of ZIF-8/Pd/ZnO NWs gas sensor to the same concentrations of H_2 gas are 3.2, 4.7 and 6.7 respectively. Even though the response of the ZIF-8-coated sensor is lower, its selectivity is considerably enhanced in comparison with those of membrane-free sensors. In fact, as it can be seen from Figure 6c, the ZIF-8/Pd/ZnO NWs gas sensor does not show any response to interfering gases did not show any noticeable response towards C_6H_6, C_7H_8, C_2H_5OH and CH_3COCH_3 gases, whereas a strong response towards H_2 gas was obtained which demonstrates its excellent selectivity, due to presence of the molecular sieve nanomembrane. In contrast, the Pd/ZnO NWs gas sensor shows an intense response of (50 ppm response of 8.5 ± 0.4) to H_2 gas, but non negligible responses to other interfering gases such as C_6H_6 (50 ppm response: 3.6 ± 0.2), C_7H_8 (50 ppm response: 3.4 ± 0.2), C_2H_5OH (50 ppm response: 2.7 ± 0.1) and CH_3COCH_3 (50 ppm response: 4.7 ±0.2). These results clearly demonstrate the weaker selectivity of the membrane-free sensor in comparison with the optimized ZIF-8/Pd/ZnO NWs gas sensor.

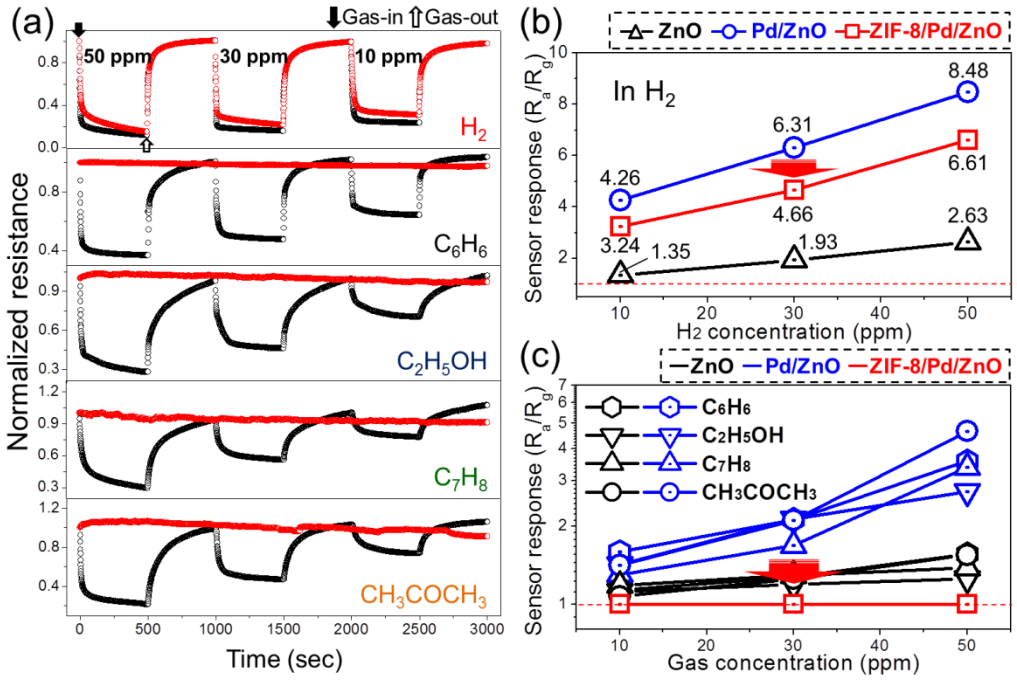

Figure 6. (a) Dynamic normalized resistance curves of Pd/ZnO and ZIF-8/Pd/ZnO NWs gas sensors to 10, 30 and 50 ppm H_2, C_6H_6, C_2H_5OH, C7H8 and CH_3COCH_3 gases. (b) Calibration curves of bare ZnO,

Pd/ZnO and ZIF-8/Pd/ZnO NWs gas sensors to 10, 30 and 50 ppm H_2 gas. (c) Calibration curves of bare ZnO, Pd/ZnO and ZIF-8/Pd/ZnO NWs gas sensors to 10, 30 and 50 ppm H_2, C_6H_6, C_2H_5OH, C_7H_8 and CH_3COCH_3 interfering gases.

Figure 7 compares the sensitivity responses of bare ZnO NWs, Pd/ZnO NWs and ZIF-8/ Pd/ZnO NWs sensors to different gases (50 ppm in air) at 200°C. This figure also clearly evidences the excellent selectivity of the ZIF-8/Pd/ZnO NWs gas sensor towards H_2 gas (the dynamic resistance curves measured for the different gases are given in Supporting Information (Figure S7).)

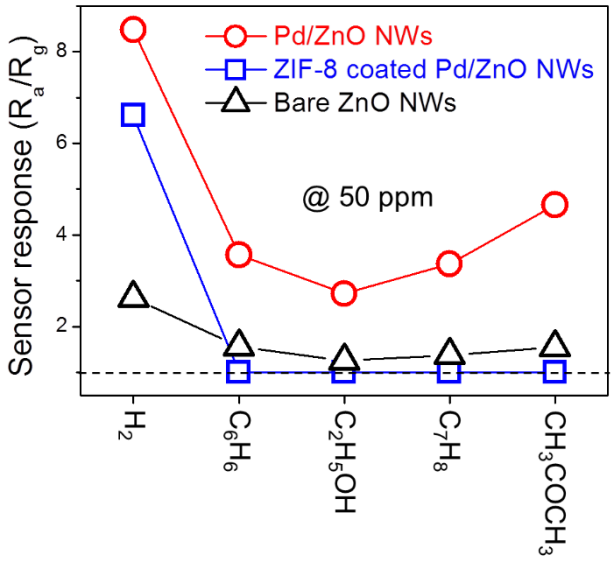

Figure 7. Sensing responses of bare ZnO NWs, Pd/ZnO NWs and ZIF-8 coated Pd/ZnO NWs gas sensors to 50 ppm of H_2, C_6H_6, C_7H_8, C_2H_5OH and CH_3COCH_3 gases in air at 200°C.

Although the response of the ZIF-8/Pd/ZnO NWs gas sensor towards H_2 gas is ~20% lower than that of Pd/ZnO NWs based sensor, its overall performance as hydrogen sensor is much better, as its selectivity clearly outperforms the other sensor designs. As already discussed in our previous work,[20] although the high adsorption capacity of MOF structures (concentration effect) contributes to increase the sensitivity toward the diffusing species, the sensor response is influenced by the diffusion limitation of H_2 through the ZIF-8 membrane which controls the access of H_2 to the ZnO

NWs surface and thus its detection rate. This causes as well a slightly lower response of ZIF-8/Pd/ZnO NWs gas sensors relative to Pd/ZnO NWs gas sensor.

This excellent selectivity is a good evidence for the impact and viability of the new sensor design. The molecular sieving properties provided by the MOF membrane enable the ZIF-8/Pd/ZnO NWs gas sensor to outperform both the Pd/ZnO NWs and the bare ZnO NWs sensing devices. In fact, due to presence of the molecular sieve membrane, only H_2 gas molecules can reach the sensing surface. It is worth noticing that the diffusion of H_2 through the ultramicroporous ZIF-8 network is a thermally activated transport mechanism and this is particularly favorable for designing a highly sensitive and selective sensor for H_2 detection at high temperature (e.g. 200-300°C). A schematic representation of the sensing mechanisms for the three gas sensors designs is provided in Figure 8.

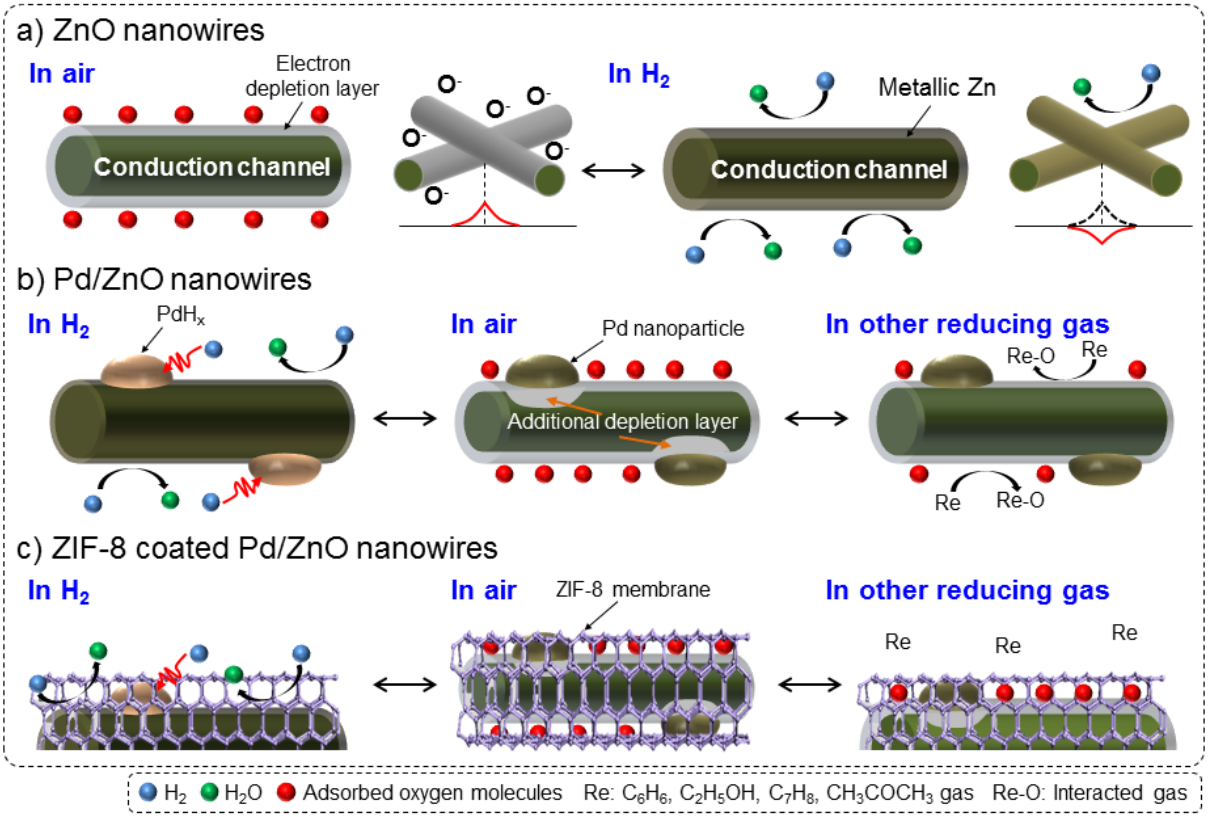

Figure 8. Schematic representation of the sensing mechanisms for (a) pristine ZnO NWs, (b) Pd/ZnO NWs and (c) ZIF-8 coated Pd/ZnO NWs sensors.

As shown in Figure 8a, when the bare ZnO NWs is initially exposed to air atmosphere, oxygen molecules are adsorbed on the oxide surface and by subsequent capture of electrons from conduction bands, a so-called electron depletion layer is generated at the surface of ZnO NWs. As a result, the electric current is confined within the conduction channel of ZnO NWs, as already discussed in our previous work.[21] In addition, because of the networked nature of ZnO NWs, the presence of ZnO-ZnO homojunctions causes the appearance of a potential barrier which is significantly high in air. Figure S8 shows the FE-SEM cross-section image of pure ZnO NWs. Due to the networked and random structure of the synthesized ZnO NWs, there are many n-ZnO/n-ZnO homojunctions. Upon exposure to H_2 gas, due to the relatively high sensing temperature, the ZnO surface is reduced to metallic Zn with much higher conductivity than ZnO.[55] Consequently, the width of conduction channel increases and at the same time, the height of barrier junctions also significantly decreases. Accordingly, the overall resistance of pristine ZnO NWs gas sensor decreases, leading to the appearance of the sensor response signal.

Due to the presence of Pd NPs, additional sensing mechanisms take place for the Pd/ZnO NWs sensors. As shown in Figure 8b, due to the difference in work functions of Pd and ZnO, electrons will transfer to ZnO upon contact to equilibrate the Fermi levels in both materials. Therefore, at the contact area between Pd and ZnO, the depth of electron depletion layer increases and this leads to a higher resistance of Pd/ZnO NWs sensor when compared to bare ZnO NWs gas sensor. Upon exposure to H_2 gas, palladium is converted to palladium hydride (PdH_x) and a part of ZnO (surface) is converted to metallic Zn.[56-57] Both mechanisms lead to higher conductivities, contributing to the sensor response signal. However, in case of exposure to other reducing gases, only the thickness of the electron depletion layer decreases, leading to lower responses of Pd/ZnO NWs to other reducing gases. By selecting the appropriate metallic NPs, the response signal could be maximized for other molecules/species as well, extending the tuning possibilities of this type of sensing device.

Finally, when considering the case of ZIF-8 coated Pd/ZnO NWs sensors (Figure 8c), the reducing gases with kinetic diameters larger than the ZIF-8 windows cannot pass through and cannot reach the metal oxide surface. Accordingly, the tested series of interfering molecules (all larger than H_2) were not able to pass through the ZIF-8 overcoat, and did not yield any sensor response signal. In addition even if the Pd NPs are not fully covered by the ZIF-8 membrane (Figure 4e), this is not really a problem as far as only hydrogen will be sorbed and transported by the Pd NPs to the ZnO surface. This also contributes to the excellent selectivity towards H_2 gas observed for the ZIF-8/Pd/ZnO NWs gas sensing device. By choosing the appropriate type of MOF overcoat, the pore sizes could be tuned, and this strategy could be extended towards the selective sensing of other gases as well.

CONCLUSION

Sensitivity and selectivity are key parameters for metal oxide-based gas sensors. In this work, we reported a novel strategy for the enhancement of both sensitivity and selectivity in gas sensing devices, applied to the detection of H_2 gas. The results obtained showed that the performance of gas sensors towards H_2 gas can be greatly increased by the addition of Pd NPs and the use of ZIF-8 coating acting as a molecular sieve membrane layer.

This novel sensor design involved the controlled growth of a MOF (ZIF-8) nanomembrane uniformly coating a sensor based on ZnO NWs decorated with Pd NPs. The Pd NPs enable the sensor to reach an intense signal response for H_2 sensing, whereas the ZIF-8 overcoat enable for an excellent selectivity. In fact, the response signal obtained for H_2 detection reached very high values, whereas no noticeable responses towards the other interfering gases tested (C_6H_6, C_7H_8, C_2H_5OH and CH_3COCH_3) could be detected, evidencing the excellent selectivity obtained with this new sensor design. In addition, by a judicious choice of both the metallic NPs and MOFs materials with tuned properties for specific molecules detection, the strategy presented could be extended to the sensing of other species. Finally, as both the ALD and the solvothermal route used for the nanocomposite

sensor preparation are scalable, they effectively enable the fabrication of fully integrated sensing devices. The proof-of-concept results presented in this work pave the way for the development of new generation of highly sensitive and selective gas nanosensors, and open a novel avenue for sensing devices technologies.

ACKNOWLEDGEMENTS

The authors are grateful to Bruno Navarra (CNRS-IEM) for his technical assistance. Campus France (Grant 29888RC- Star 2013) and the European Institute of Membranes of Montpellier (exploratory project COMET-MOF- "Next Generation Membranes"- Internal IEM Call 2015) are acknowledged for funding. This research study was also supported by the French National Agency (ANR, program MeNiNA - ANR-17-CE09-0049) and by Basic Science Research Program through the National Research Foundation of Korea (NRF) funded by the Ministry of Education (2016R1D1A1B03935228).

AUTHOR INFORMATION

Corresponding Authors

*E-mail: mikhael.bechelany@univ-montp2.fr. Phone: +33467149167. Fax: +33467149119.

*E-mail: Kim:sangsub@inha.ac.kr. Phone: +82328607546. Fax: +82328625546.

Author Contributions

† M.W. and J.-H.K. contributed equally to this work.

SUPPORTING INFORMATION

S1 : XPS surveys ; S2 : TEM images of the ZIF-8/Pd/ZnO NWs sensing nanomaterials ; S3 : XRD patterns ; S4 : Thermogravimetric analysis ; S5 : Dynamic resistance curves of bare ZnO NWs gas

sensor as function of temperature; S6 : Dynamic resistance curves of Pd/ZnO NWs gas sensor as function of temperature ; S7 : Dynamic resistance curves of the gas sensors measured for various gases ; S8 : SEM images of bare ZnO NWs.

REFERENCES

1. Korotcenkov, G.; Han, S. D.; Stetter, J. R. Review of electrochemical hydrogen sensors. *Chemical Reviews* **2009,** *109*, 1402-1433.
2. Sasaki, K. Why Hydrogen? Why Fuel Cells? In *Hydrogen Energy Engineering*, Springer: **2016**, pp 3-14.
3. Hübert, T.; Boon-Brett, L.; Black, G.; Banach, U. Hydrogen sensors–a review. *Sensors and Actuators B: Chemical* **2011,** *157*, 329-352.
4. Gu, H.; Wang, Z.; Hu, Y. Hydrogen gas sensors based on semiconductor oxide nanostructures. *Sensors* **2012,** *12*, 5517-5550.
5. Wang, C.; Yin, L.; Zhang, L.; Xiang, D.; Gao, R. Metal oxide gas sensors: sensitivity and influencing factors. *Sensors* **2010,** *10*, 2088-2106.
6. Aroutiounian, V. Metal oxide hydrogen, oxygen, and carbon monoxide sensors for hydrogen setups and cells. *International Journal of Hydrogen Energy* **2007,** *32*, 1145-1158.
7. Eranna, G.; Joshi, B.; Runthala, D.; Gupta, R. Oxide materials for development of integrated gas sensors—a comprehensive review. *Critical Reviews in Solid State and Materials Sciences* **2004,** *29*, 111-188.
8. Li, S.-J.; Bao, D.; Shi, M.-M.; Wulan, B.-R.; Yan, J.-M.; Jiang, Q. Amorphizing of Au Nanoparticles by CeOx–RGO Hybrid Support towards Highly Efficient Electrocatalyst for N2 Reduction under Ambient Conditions. *Advanced Materials* **2017,** *29*, 1700001.
9. Yan, J.-M.; Li, S.-J.; Yi, S.-S.; Wulan, B.-R.; Zheng, W.-T.; Jiang, Q. Anchoring and Upgrading Ultrafine NiPd on Room-Temperature-Synthesized Bifunctional NH2-N-rGO toward Low-Cost and Highly Efficient Catalysts for Selective Formic Acid Dehydrogenation. *Advanced Materials* **2018,** *30*, 1703038.
10. Wang, Y.; Cao, J.; Qin, C.; Zhang, B.; Sun, G.; Zhang, Z. Synthesis and Enhanced Ethanol Gas Sensing Properties of the g-C(3)N(4) Nanosheets-Decorated Tin Oxide Flower-Like Nanorods Composite. *Nanomaterials* **2017,** *7*, 285.
11. Ju, D.-X.; Xu, H.-Y.; Qiu, Z.-W.; Zhang, Z.-C.; Xu, Q.; Zhang, J.; Wang, J.-Q.; Cao, B.-Q. Near Room Temperature, Fast-Response, and Highly Sensitive Triethylamine Sensor Assembled with Au-Loaded ZnO/SnO2 Core–Shell Nanorods on Flat Alumina Substrates. *Acs Applied Materials & Interfaces* **2015,** *7*, 19163-19171.
12. Shi, M.-M.; Bao, D.; Wulan, B.-R.; Li, Y.-H.; Zhang, Y.-F.; Yan, J.-M.; Jiang, Q. Au Sub-Nanoclusters on TiO2 toward Highly Efficient and Selective Electrocatalyst for N2 Conversion to NH3 at Ambient Conditions. *Advanced Materials* **2017,** *29*, 1606550.
13. Duan, Y.-X.; Meng, F.-L.; Liu, K.-H.; Yi, S.-S.; Li, S.-J.; Yan, J.-M.; Jiang, Q. Amorphizing of Cu Nanoparticles toward Highly Efficient and Robust Electrocatalyst for CO2 Reduction to Liquid Fuels with High Faradaic Efficiencies. *Advanced Materials* **2018,** *30*, 1706194.

14. Shi, M.-M.; Bao, D.; Li, S.-J.; Wulan, B.-R.; Yan, J.-M.; Jiang, Q. Anchoring PdCu Amorphous Nanocluster on Graphene for Electrochemical Reduction of N2 to NH3 under Ambient Conditions in Aqueous Solution. *Advanced Energy Materials* **2018,** *8*, 1800124.
15. Wang, H.-T.; Kang, B.; Ren, F.; Tien, L.; Sadik, P.; Norton, D.; Pearton, S.; Lin, J. Hydrogen-selective sensing at room temperature with ZnO nanorods. *Applied Physics Letters* **2005,** *86*, 243503.
16. Lupan, O.; Ursaki, V.; Chai, G.; Chow, L.; Emelchenko, G.; Tiginyanu, I.; Gruzintsev, A.; Redkin, A. Selective hydrogen gas nanosensor using individual ZnO nanowire with fast response at room temperature. *Sensors and Actuators B: Chemical* **2010,** *144*, 56-66.
17. Ümit, Ö.; Hofstetter, D.; Morkoc, H. ZnO devices and applications: a review of current status and future prospects. *Proceedings of the IEEE* **2010,** *98*, 1255-1268.
18. Kim, I.-D.; Rothschild, A.; Tuller, H. L. Advances and new directions in gas-sensing devices. *Acta materialia* **2013,** *61*, 974-1000.
19. Drobek, M.; Bechelany, M.; Vallicari, C.; Abou Chaaya, A.; Charmette, C.; Salvador-Levehang, C.; Miele, P.; Julbe, A. An innovative approach for the preparation of confined ZIF-8 membranes by conversion of ZnO ALD layers. *Journal of Membrane Science* **2015,** *475*, 39-46.
20. Drobek, M.; Kim, J.-H.; Bechelany, M.; Vallicari, C.; Julbe, A.; Kim, S. S. MOF-Based Membrane Encapsulated ZnO Nanowires for Enhanced Gas Sensor Selectivity. *Acs Applied Materials & Interfaces* **2016,** *8*, 8323-8328.
21. Drobek, M.; Kim, J.-H.; Bechelany, M.; Vallicari, C.; Leroy, E.; Julbe, A.; Kim, S. S. Design and fabrication of highly selective H2 sensors based on SIM-1 nanomembrane-coated ZnO nanowires. *Sensors and Actuators B: Chemical* **2018,** *264*, 410-418.
22. Koo, W.-T.; Qiao, S.; Ogata, A. F.; Jha, G.; Jang, J.-S.; Chen, V. T.; Kim, I.-D.; Penner, R. M. Accelerating Palladium Nanowire H2 Sensors Using Engineered Nanofiltration. *ACS Nano* **2017,** *11*, 9276-9285.
23. Lim, Y.; Lee, Y.; Heo, J.-I.; Shin, H. Highly sensitive hydrogen gas sensor based on a suspended palladium/carbon nanowire fabricated via batch microfabrication processes. *Sensors and Actuators B: Chemical* **2015,** *210*, 218-224.
24. Chen, Z.; Jie, J.; Luo, L.; Wang, H.; Lee, C.; Lee, S. Applications of silicon nanowires functionalized with palladium nanoparticles in hydrogen sensors. *Nanotechnology* **2007,** *18*, 345502.
25. Park, J. Y.; Song, D. E.; Kim, S. S. An approach to fabricating chemical sensors based on ZnO nanorod arrays. *Nanotechnology* **2008,** *19*, 105503.
26. Holade, Y.; Hickey, D. P.; Minteer, S. D. Halide-regulated growth of electrocatalytic metal nanoparticles directly onto a carbon paper electrode. *Journal of Materials Chemistry A* **2016,** *4*, 17154-17162.
27. Cui, Z.; Li, L.; Manthiram, A.; Goodenough, J. B. Enhanced Cycling Stability of Hybrid Li–Air Batteries Enabled by Ordered Pd3Fe Intermetallic Electrocatalyst. *Journal of the American Chemical Society* **2015,** *137*, 7278-7281.
28. Cheng, N.; Shao, Y.; Liu, J.; Sun, X. Electrocatalysts by atomic layer deposition for fuel cell applications. *Nano Energy* **2016,** *29*, 220-242.
29. Kosimaningrum, W. E.; Le, T. X. H.; Holade, Y.; Bechelany, M.; Tingry, S.; Buchari, B.; Noviandri, I.; Innocent, C.; Cretin, M. Surfactant- and Binder-Free Hierarchical Platinum Nanoarrays Directly Grown onto a Carbon Felt Electrode for Efficient Electrocatalysis. *Acs Applied Materials & Interfaces* **2017,** *9*, 22476-22489.
30. de Jong, K. P. *Synthesis of solid catalysts*. John Wiley & Sons: **2009**.
31. Agrafiotis, C.; Tsetsekou, A.; Stournaras, C.; Julbe, A.; Dalmazio, L.; Guizard, C.; Boretto, G.; Debenedetti, M.; Parussa, F. Evaluation of sol–gel methods for the synthesis of doped-ceria environmental catalysis systems: Part II. Catalytic activity and resistance to thermal aging. *Applied Catalysis B: Environmental* **2001,** *34*, 149-159.
32. Siegel, R. W. Nanophase materials: synthesis, structure, and properties. In *Physics of new materials*, Springer: **1994**, pp 65-105.
33. Marichy, C.; Bechelany, M.; Pinna, N. Atomic Layer Deposition of Nanostructured Materials for Energy and Environmental Applications. *Advanced Materials* **2012,** *24*, 1017-1032.

34. Leick, N.; Weber, J.; Mackus, A.; Weber, M.; van de Sanden, M.; Kessels, W. In situ spectroscopic ellipsometry during atomic layer deposition of Pt, Ru and Pd. *Journal of Physics D: Applied Physics* **2016,** *49*, 115504.
35. George, S. M. Atomic Layer Deposition: An Overview. *Chemical Reviews* **2010,** *110*, 111-131.
36. Leskelä, M.; Ritala, M. Atomic layer deposition (ALD): from precursors to thin film structures. *Thin solid films* **2002,** *409*, 138-146.
37. Weber, M. J.; Verheijen, M. A.; Bol, A. A.; Kessels, W. M. M. Sub-nanometer dimensions control of core/shell nanoparticles prepared by atomic layer deposition. *Nanotechnology* **2015,** *26*, 094002.
38. Weber, M. J.; Mackus, A. J. M.; Verheijen, M. A.; van der Marel, C.; Kessels, W. M. M. Supported Core/Shell Bimetallic Nanoparticles Synthesis by Atomic Layer Deposition. *Chemistry of Materials* **2012,** *24*, 2973-2977.
39. Rikkinen, E.; Santasalo-Aarnio, A.; Airaksinen, S.; Borghei, M.; Viitanen, V.; Sainio, J.; Kauppinen, E. I.; Kallio, T.; Krause, A. O. I. Atomic layer deposition preparation of Pd nanoparticles on a porous carbon support for alcohol oxidation. *The Journal of Physical Chemistry C* **2011,** *115*, 23067-23073.
40. Assaud, L.; Brazeau, N.; Barr, M. K. S.; Hanbucken, M.; Ntais, S.; Baranova, E. A.; Santinacci, L. Atomic Layer Deposition of Pd Nanoparticles on TiO2 Nanotubes for Ethanol Electrooxidation: Synthesis and Electrochemical Properties. *Acs Applied Materials & Interfaces* **2015,** *7*, 24533-24542.
41. Adriaan, J. M. M.; Matthieu, J. W.; Nick, F. W. T.; Diana, G.-A.; René, H. J. V.; Simone, A.; Ageeth, A. B.; Marcel, A. V.; Wilhelmus, M. M. K. Atomic layer deposition of Pd and Pt nanoparticles for catalysis: on the mechanisms of nanoparticle formation. *Nanotechnology* **2016,** *27*, 034001.
42. Weber, M. J.; Mackus, A. J. M.; Verheijen, M. A.; Longo, V.; Bol, A. A.; Kessels, W. M. M. Atomic Layer Deposition of High-Purity Palladium Films from Pd(hfac)2 and H2 and O2 Plasmas. *The Journal of Physical Chemistry C* **2014,** *118*, 8702-8711.
43. Park, J. Y.; Park, Y. K.; Kim, S. S. Formation of networked ZnO nanowires by vapor phase growth and their sensing properties with respect to CO. *Materials Letters* **2011,** *65*, 2755-2757.
44. Weber, M.; Koonkaew, B.; Balme, S.; Utke, I.; Picaud, F.; Iatsunskyi, I.; Coy, E.; Miele, P.; Bechelany, M. Boron Nitride Nanoporous Membranes with High Surface Charge by Atomic Layer Deposition. *Acs Applied Materials & Interfaces* **2017,** *9*, 16669-16678.
45. Matthieu, W.; Philippe, C.; Hoda, E. G.; Sophie, T.; Mikhael, B.; Yaovi, H. Enhanced Catalytic Glycerol Oxidation Activity Enabled by Activated-Carbon-Supported Palladium Catalysts Prepared through Atomic Layer Deposition. *ChemElectroChem* **2018,** *5*, 743-747.
46. Bechelany, M.; Drobek, M.; Vallicari, C.; Abou Chaaya, A.; Julbe, A.; Miele, P. Highly crystalline MOF-based materials grown on electrospun nanofibers. *Nanoscale* **2015,** *7*, 5794-5802.
47. Chen, L.; Peng, Y.; Wang, H.; Gu, Z.; Duan, C. Synthesis of Au@ZIF-8 single- or multi-core–shell structures for photocatalysis. *Chemical Communications* **2014,** *50*, 8651-8654.
48. Sun, G.-J.; Choi, S.-W.; Katoch, A.; Wu, P.; Kim, S. S. Bi-functional mechanism of H2S detection using CuO-SnO2 nanowires. *Journal of Materials Chemistry C* **2013,** *1*, 5454-5462.
49. Choi, S.-W.; Katoch, A.; Sun, G.-J.; Kim, J.-H.; Kim, S.-H.; Kim, S. S. Dual Functional Sensing Mechanism in SnO2–ZnO Core–Shell Nanowires. *Acs Applied Materials & Interfaces* **2014,** *6*, 8281-8287.
50. Hermes, S.; Schröder, F.; Chelmowski, R.; Wöll, C.; Fischer, R. A. Selective Nucleation and Growth of Metal−Organic Open Framework Thin Films on Patterned COOH/CF3-Terminated Self-Assembled Monolayers on Au(111). *Journal of the American Chemical Society* **2005,** *127*, 13744-13745.
51. Xu, X.; Lu, Y.; Yang, Y.; Nosheen, F.; Wang, X. Tuning the growth of metal-organic framework nanocrystals by using polyoxometalates as coordination modulators. *Science China Materials* **2015,** *58*, 370-377.
52. Maina, J. W.; Schütz, J. A.; Grundy, L.; Des Ligneris, E.; Yi, Z.; Kong, L.; Pozo-Gonzalo, C.; Ionescu, M.; Dumée, L. F. Inorganic Nanoparticles/Metal Organic Framework Hybrid Membrane

Reactors for Efficient Photocatalytic Conversion of CO2. *Acs Applied Materials & Interfaces* **2017,** *9*, 35010-35017.
53. Gražulis, S.; Chateigner, D.; Downs, R. T.; Yokochi, A. F. T.; Quirós, M.; Lutterotti, L.; Manakova, E.; Butkus, J.; Moeck, P.; Le Bail, A. Crystallography Open Database – an open-access collection of crystal structures. *Journal of Applied Crystallography* **2009,** *42*, 726-729.
54. Sun, Y. E.; Zhang, D. Z.; Chang, H. Y.; Zhang, Y. Fabrication of palladium-zinc oxide-reduced graphene oxide hybrid for hydrogen gas detection at low working temperature. *Journal of Materials Science-Materials in Electronics* **2017,** *28*, 1667-1673.
55. Gaspar, D.; Pereira, L.; Gehrke, K.; Galler, B.; Fortunato, E.; Martins, R. High mobility hydrogenated zinc oxide thin films. *Solar Energy Materials and Solar Cells* **2017,** *163*, 255-262.
56. Baek, J.; Jang, B.; Kim, M. H.; Kim, W.; Kim, J.; Rim, H. J.; Shin, S.; Lee, T.; Cho, S.; Lee, W. High-performance hydrogen sensing properties and sensing mechanism in Pd-coated p-type Si nanowire arrays. *Sensors and Actuators B: Chemical* **2018,** *256*, 465-471.
57. Esfandiar, A.; Irajizad, A.; Akhavan, O.; Ghasemi, S.; Gholami, M. R. Pd–WO3/reduced graphene oxide hierarchical nanostructures as efficient hydrogen gas sensors. *International Journal of Hydrogen Energy* **2014,** *39*, 8169-8179.